catalysts

MDPI

Article

Solid–Waste–Derived Geopolymer–Type Zeolite–like High Functional Catalytic Materials Catalyze Efficient Hydrogenation of Levulinic Acid

Wenli Feng [1], Xuebin Lu [1,2], Jian Xiong [1], Zhihao Yu [2], Yilin Wang [1], Jianguo Cui [1], Rui Zhang [3,*] and Rengui Weng [4,*]

[1] School of Science, Tibet University, Lhasa 850000, China
[2] School of Environmental Science and Engineering, Tianjin University, Tianjin 300350, China
[3] School of Environmental and Municipal Engineering, Tianjin Chengjian University, Tianjin 300384, China
[4] College of Ecological Environment and Urban Construction, Fujian University of Technology, Fuzhou 350118, China
* Correspondence: rzhang@tcu.edu.cn (R.Z.); wengrengui109@126.com (R.W.)

Abstract: Three common solid wastes (waste incineration fly ash, sewage sludge, and polluted soil) were the raw materials used in the synthesis of a geopolymer–type zeolite–like product, which was then used as a catalyst carrier to prepare a nickel hydrogenation catalyst for the catalytic hydrogenation of levulinic acid to γ–valerolactone. Under optimum synthesis conditions, the synthesized geopolymer zeolite has excellent structure and performance. The characterization results show that the composites have a three–dimensional network structure, and the pore structure is homogeneous mesoporous or microporous. In this work, the results of catalytic hydrogenation show that the yield of γ–valerolactone can achieve up to 94% using the synthesized catalyst, which is comparable to that of commercial catalysts and the concentrations of typical polluting heavy metals of Cu, Zn, Pb, and Cd in the reaction solution were all below the emission concentration limit (Class I standard) after five cycles of reaction. In summary, this geopolymer–type zeolite–like catalyst is cheap and has excellent performance; it is, therefore, expected to be widely used in catalysis instead of commercial carriers.

Keywords: geopolymer–type zeolite–like catalyst; levulinic acid; hydrogenation

Citation: Feng, W.; Lu, X.; Xiong, J.; Yu, Z.; Wang, Y.; Cui, J.; Zhang, R.; Weng, R. Solid–Waste–Derived Geopolymer–Type Zeolite–like High Functional Catalytic Materials Catalyze Efficient Hydrogenation of Levulinic Acid. *Catalysts* **2022**, *12*, 1361. https://doi.org/10.3390/catal12111361

Academic Editors: Isabel Santos-Vieira and Mário Manuel Quialheiro Simões

Received: 24 September 2022
Accepted: 28 October 2022
Published: 4 November 2022

1. Introduction

Economic growth drives levels of urbanization and industrialization to increase, thereby leading to an increase in the amount of solid waste generated around the world [1,2]. Because a considerable amount of solid waste is highly toxic, flammable, explosive, and highly corrosive, improper handling can cause serious harm to the environment and the health of humans. At the same time, the discharge and disposal of solid waste also result in huge economic losses [1,3]. Therefore, finding a reasonable way to harmlessly dispose of solid waste is currently of great interest. At present, resource utilization of solid waste is the first choice for the harmless disposal of solid waste because it can generate economic benefits while purifying the waste [4].

In 1972, Davidovits originally developed "Geopolymer"—a crystalline aluminosilicate material with a three–dimensional network structure composed of a silicon–oxygen tetrahedron and an aluminum–oxygen tetrahedron bridged by oxygen atoms [5,6]. In theory, materials rich in silicon and aluminum, such as waste incineration fly ash, sewage sludge, etc., can be used as the raw materials in the synthesis of geopolymers. Due to its specific physicochemical structure (three–dimensional cage–like composition structure and the widespread presence of negative charges of alumina tetrahedron), geopolymer has the function of fixing and stabilizing toxic and harmful elements in solid waste; it also has good durability, thermal stability, acid and alkali corrosion resistance, and structural properties similar to zeolite. However, it has the problems of poor porosity and low mass

transfer efficiency, which limit its wide application, so it is mainly used in low value–added fields such as building materials and fillers [7,8]. Researchers, therefore, began to use various methods to introduce pores into geopolymers; current commonly used methods for introducing pores include the embedded filler method, sacrificial template method, 3D printing method, and direct foaming method [9–13]. Of these, the direct foaming method is widely used as it is simple and cheap. In the direct foaming method, both the ratio of alkali activator to foaming agent and the ratio of silicon to aluminum in polymer slurry are important factors affecting product performance [14]. In summary, geopolymer–type zeolite–like high–functional materials can be synthesized from solid wastes rich in silicon and aluminum, and the structure of geopolymer products can be designed and optimized by tuning external additives.

Biomass–based compounds are an important sustainable resource which have great potential in the field of energy production. Biomass–based compound γ–valerolactone (GVL) attracted much attention due to its excellent physicochemical properties, such as high energy value and low vapor pressure, and its use as an ideal fuel additive. Levulinic acid (LA) is the most common substrate for the synthesis of GVL, due to its relative cheapness and availability [15]. Among the catalysts for the hydrogenation of LA to GVL, nickel non–precious metal catalysts are the most commonly used metal catalysts due to their cheapness, availability, and high activity [16–19]. Studies showed that catalysts synthesized by different supports supported by nickel have different catalytic effects; the support mainly affects the catalytic effect by affecting the dispersion of metal particles and the binding effect of the metal support [20–22]. At present, materials with high stability, such as commercial silica and zeolite, etc., are mainly used as supports for nickel catalysts. However, the above–mentioned catalytic support materials have the disadvantage of being expensive; this hinders the large–scale industrial use of catalysts so the development of inexpensive and high–performance catalytic support materials is urgently needed [18,20,23]. The geopolymer–type zeolite–like material derived from solid waste is cheap, stable, excellent in structure (similar to zeolite), and highly controllable in pore size, giving it great potential as an excellent catalytic carrier.

To sum up, this research aims to make use of solid wastes as a resource to synthesize highly functional materials. The purpose is to broaden the way solid wastes can be used as a resource, and to improve their utilization rate. At the same time, the research provides a new perspective for the construction of new catalytic materials. In this research, several common solid wastes rich in silicon and aluminum (waste incineration fly ash (WIFA), sewage sludge (SPS), and polluted soil following the high temperature treatment of pesticide plants (PFPS)) were taken as the research objects; metakaolin (MK) was used as the typical control raw material for synthesizing geopolymers. The geopolymer–type zeolite–like product was synthesized and then used as a catalyst carrier in the hydrogenation process for the preparation of GVL by LA, under high–temperature and high–pressure conditions, in order to test catalyst and carrier performance.

2. Results and Discussion

2.1. Preparation of Geopolymer–Type Zeolite–Like Products

Figure 1a shows the isotherm adsorption–desorption curves of the GC–MK1~7 series of products under different ratios and dosages of alkali activators. The observed images show that all samples exhibit the IV–type curve characteristics, and a magnetic hysteresis loop appears, which proves that the prepared products all have mesoporous structures. Observing Table 1, it is found that the specific surface area of the GC–MK1~3 series of products first increases and then decreases, and the average pore size first increases and then remains unchanged; GC–MK2 has the best structural properties. This shows that a good reagent ratio of potassium silicate to potassium hydroxide is 1:1, and the lack of silicon or alkali would not be conducive to a good product structure. This is because the lack of alkali may inhibit the dissolution of silicon and aluminum in the feedstock, while the lack of silicon leads to incomplete polymerization, thereby inhibiting the formation

of zeolite structures; it also inhibits the in–situ foaming reaction with hydrogen peroxide due to the lack of reactant silicon [13,24]. Observing Table 1, it is found that with the increase in the proportion of silicate solution in the alkali activator, the specific surface area of the GC–MK4~7 series of products shows an upward trend, and the rising trend slows down in the later period, reaching its maximum value in GC–MK7. In addition, the average pore size of the product first increased and then decreased, reaching a maximum in GC–MK6. This may be due to the fact that the polymerization reaction reached a dynamic equilibrium in the later stage, and the continued addition of silicate no longer promoted the reaction, but existed in the system in a free state; the excess silicate is, therefore, not conducive to effective product structure performance [24,25]. Figure 2a is the pore diameter distribution diagram; it can be seen from the image that the pore size distribution of GC–MK4~7 geopolymer–type zeolite–like products all show bimodal characteristics. With the increase in silicate solution content, the peak value gradually shifts to the right. Generally speaking, the lower the density grade, the larger the bubble pore size; a large amount of potassium silicate solution will increase the water content of the slurry, reduce the density of the slurry, and cause the pore diameter to move to a larger value [26–28].

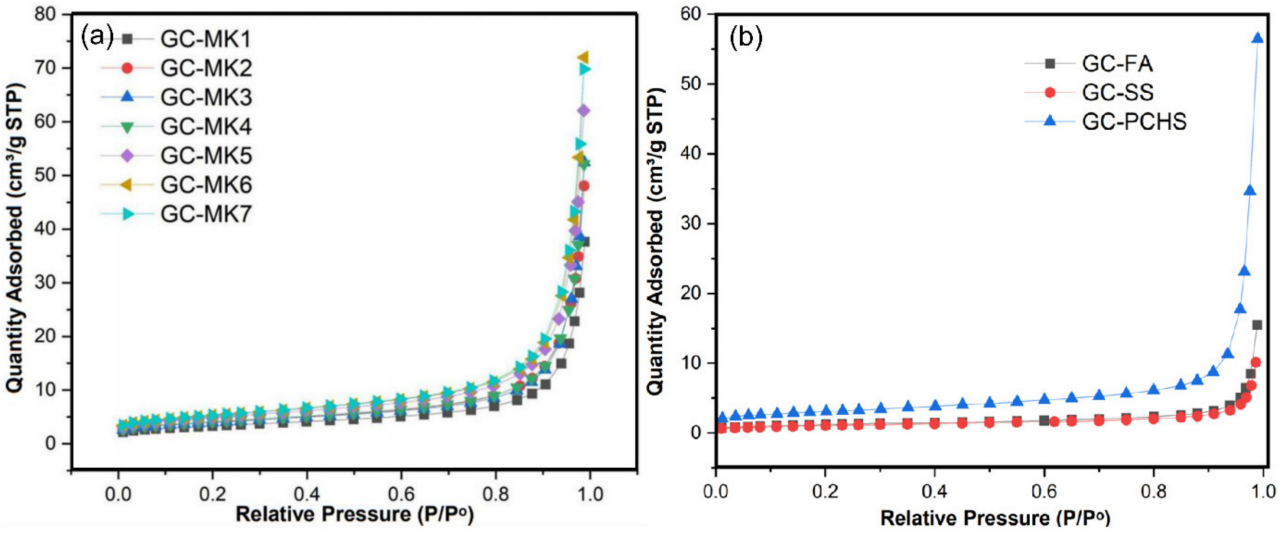

Figure 1. Isothermal adsorption–desorption curves of geopolymer–type zeolite–like products derived from different raw materials. (**a**) GC–MK 1~7, (**b**) GC–WIFA, GC–SPS, GC–PFPS.

Table 1. Physical adsorption test data.

	GC–MK1	GC–MK2	GC–MK3	GC–MK4	GC–MK5	GC–MK6	GC–MK7	GC–WIFA	GC–SPS	GC–PFPS
Specific surface area (m^2/g)	11.53	13.92	13.81	14.44	17.08	18.38	18.56	4.29	10.72	3.80
Pore size (nm)	18.64	20.24	20.24	21.38	21.85	22.89	22.64	22.27	32.61	16.48
Pore volume (cm^3/g)	0.054	0.070	0.076	0.077	0.093	0.110	0.110	0.024	0.087	0.015

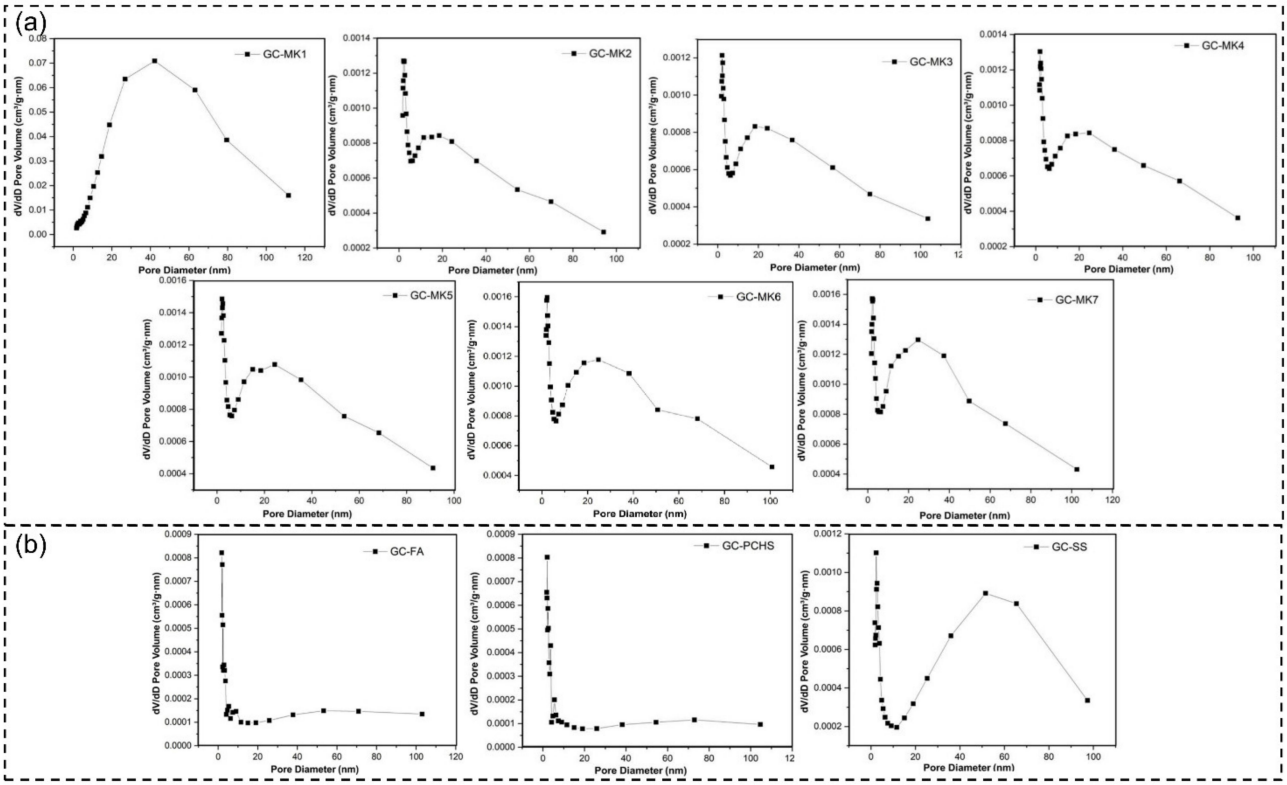

Figure 2. The pore size distribution patterns of geopolymer–type zeolite–like products derived from different raw materials. (**a**) are GC–MK 1~7, (**b**) are GC–WIFA, GC–SPS, GC–PFPS.

In summary, the synthesis methods used for GC–MK6 and GC–MK7 are better. Considering the relatively small content of silicon and aluminum components in solid waste, the proportions of alkali activators are selected as follows: 40 wt% KOH solution (11 mol/L) and 80 wt% K_2SiO_3 solution (99%).

Based on the above research, different solid wastes were used as raw materials, to explore the effect of raw material composition on the structure of geopolymer–type zeolite–like products. Figure 1b shows the isotherm adsorption–desorption curves of different solid waste–based geopolymer–type zeolite–like products; the adsorption–desorption isotherm curve of GC–SPS exhibits the characteristics of a type IV curve, and a hysteresis loop appears, indicating that it has a mesoporous structure; the curve characteristics of GC–PFPS and GC–WIFA are closer to the type I curve, and activated carbon or zeolite–like products with a microporous structure are often present in this type. Figure 2b and Table 1 show that the pore diameter distribution of GC–SPS exhibits a bimodal distribution, the peaks appearing at about 2.33 and 51.38 nm, whereas GC–PFPS and GC–WIFA display approximately normal distribution, their peaks being in the micropore range. The pore structure of synthetic samples with different raw materials are different, indicating that the raw materials have a certain influence on the structure of the product, and further analysis, in combination with characterization, is required.

SEM tests were performed on GC–MK7, GC–WIFA, GC–SPS, and GC–PFPS. The results are shown in Figure 3. It was found that the four samples all had the surface structure of fine particle agglomerates. The surface morphology of GC–MK7 was the most dense, with a small amount of granular substances distributed on the surface. GC–WIFA is formed by the aggregation of small particles of uneven shape and size, with a loose structure and rough surface. The GC–SPS structure is mainly composed of fine round particles with pores of different sizes distributed on the surface, while the GC–PFPS is mainly composed of rod–shaped particles connected to form a honeycomb structure with the highest degree of looseness. Figure 3 and Table 1 show that with the increase in

the silicon content in the raw materials, the sample presents a more uniform and dense microstructure, the particle agglomeration is more dense, and the surface connection is smoother, indicating that the existence of a sufficient amount of silicon is beneficial to the polymerization reaction and product performance.

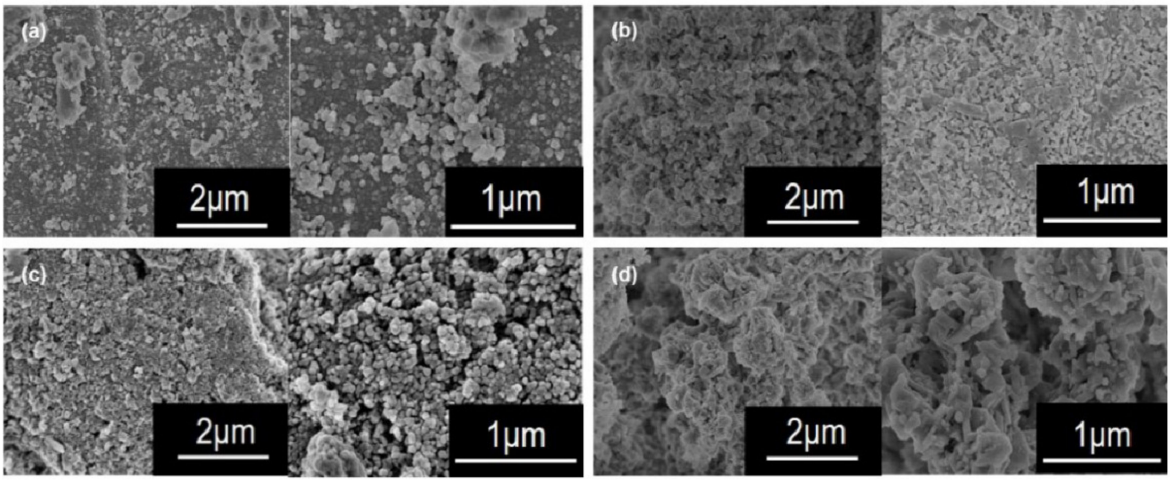

Figure 3. SEM images of geopolymer–type zeolite–like products derived from different raw materials. (**a**) GC–MK7, (**b**) GC–WIFA, (**c**) GC–SPS, (**d**) GC–PFPS.

The chemical bond structure of the material molecules was analyzed by FTIR, as shown in Figure 4. The peaks of the four products at 1113~1009 cm^{-1} are generated by the stretching vibration of Si–O–Si, and the ascending peak order is GC–PFPS (1009.42 cm^{-1}) < GC–MK7 (1058.98 cm^{-1}) < GC–WIFA (1113.24 cm^{-1}) < GC–SPS (1113.80 cm^{-1}). In particular, it was found that the GC–FA sample has a spectral band at 980cm^{-1}, which conforms to the asymmetric tensile vibration of Si–O–T (T=Al or Si). The shift in the absorption peak is mainly related to the change of material structure or component doping, indicating that there are some differences in the structure of geopolymers derived from different types of solid wastes. T–O–T (T is silicon or aluminum) is the chemical–bonding form of the geopolymer–type zeolite–like framework, so the appearance of this peak represents the successful formation of the geopolymer–type zeolite–like three–dimensional silica–alumina framework. The main chemical bond type in the silica–alumina framework determines the strength and durability of the product; the Si–O–Si bond is the strongest chemical bonding form, so the higher the peak strength of the product Si–O–Si bond, the higher the chemical bonding stability of the product [24,29,30]. In addition, observation of the spectra found that all four products have a band at 1634 cm^{-1}, which is consistent with the bending vibration of hydroxide; this may be related to the coverage of weakly bonded water molecules on the surface or pores of the materials. The absorption bands at 1466~1415 cm^{-1} of the four samples are consistent with the stretching vibration of the O–C–O bond; the O–C–O bond may be related to carbonate compounds, which come from the carbonation reaction of free potassium silicate and potassium hydroxide in the system [31]. The absorption band of GC–PFPS is the strongest in this range. Research shows that excessive water molecules and carbonic acid compounds in geopolymer will damage the stability of materials. In summary, the performance of the above products needs to be further determined in combination with experiments.

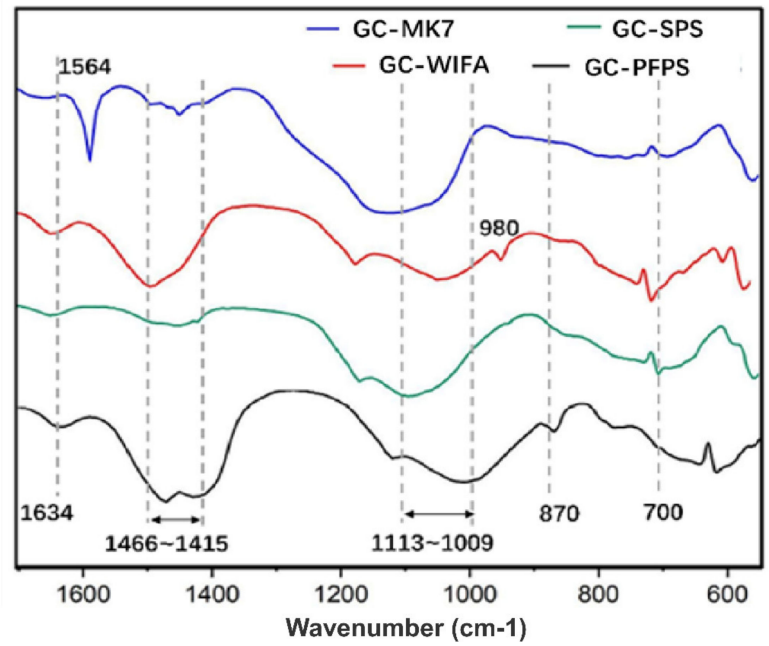

Figure 4. FTIR patterns of GC–MK7, GC–WIFA, GC–SPS, GC–PFPS.

2.2. Catalyst Performance Characterization

The four catalysts, NiO–GC–MK7, NiO–GC–WIFA, NiO–GC–SPS and NiO–GC–PFPS prepared after the modification of supported nickel, were characterized. The SEM test chart is shown in Figure 5. It was found that the original agglomerated morphology of the material still exists after modification; the surface morphology of NiO–GC–MK7, NiO–GC–WIFA, and NiO–GC–SPS is almost unchanged. The structure of NiO–GC–PFPS collapses more seriously and the previous honeycomb structure disappears, showing a smoother surface. The SEM chart and the FITR test results suggest this is possibly due to the lack of high–strength Si–O–Si bonds in the structure and the material's low resistance to high temperature. Observing the regularity of element distribution, it was found that the distribution of silicon, aluminum, and nickel on NiO–GC–MK7 and NiO–GC–WIFA is relatively uniform and dense, while the element distribution on NiO–GC–SPS and NiO–GC–PFPS is relatively scattered. This latter finding may result from the silicon–aluminum frameworks of NiO–GC–MK7 and NiO–GC–WIFA support materials being more complete, meaning the element distribution is uniform. Previous research shows that the more homogeneous the distribution of active metals, the more sufficient the contact between active centers and reactants, and the higher the catalytic effect [20,22,23].

The FTIR test of the catalyst showed that the peak distribution of the material did not change significantly. This indicates that the structure of the geopolymer–type zeolite–like product after nickel modification and high temperature calcination did not change significantly, proving that the product has high stability and high temperature resistance. XRD tests were performed on the four raw materials and nickel–loaded GC samples. Combined with Figure 6 and Table 2, it can be found that the results are shown in Figure 6: the images show that four different types of feedstock–derived catalysts have distinct peaks at 52 (2θ), corresponding to metallic nickel (JCPDS 1–1260) and indicating successful loading of metallic nickel. The 26~28 (2θ) diffraction peaks of the four samples correspond to quartz, and the 35.15 (2θ), 43.34 (2θ), and 57.49 (2θ) diffraction peaks correspond to corundum. Of these, the corundum crystal peak area of NiO–GC–MK7 is the largest. According to Table 2 and Figure 6, the formation of crystal phase of corundum may be related to more aluminum content in raw materials, research shows that the higher the ratio of silicon to aluminum, the easier it is to promote the transformation of mullite to the corundum crystal phase [29]. In addition, except for NiO–GC–MK7, the other three samples have calcium compound diffraction peaks at 27.94~30.26 (2θ). It is proved that the

Ca^{2+} in the raw material dissolves and participates in the reaction. Studies showed that, after participation in the polymerization reaction, Ca^{2+} mainly generates C–(A)–S–H gel which can be used as micro–aggregates to fill the pores of materials, promote the formation of dense structures, enhance the stability of materials, and increase the specific surface area of the material [29].

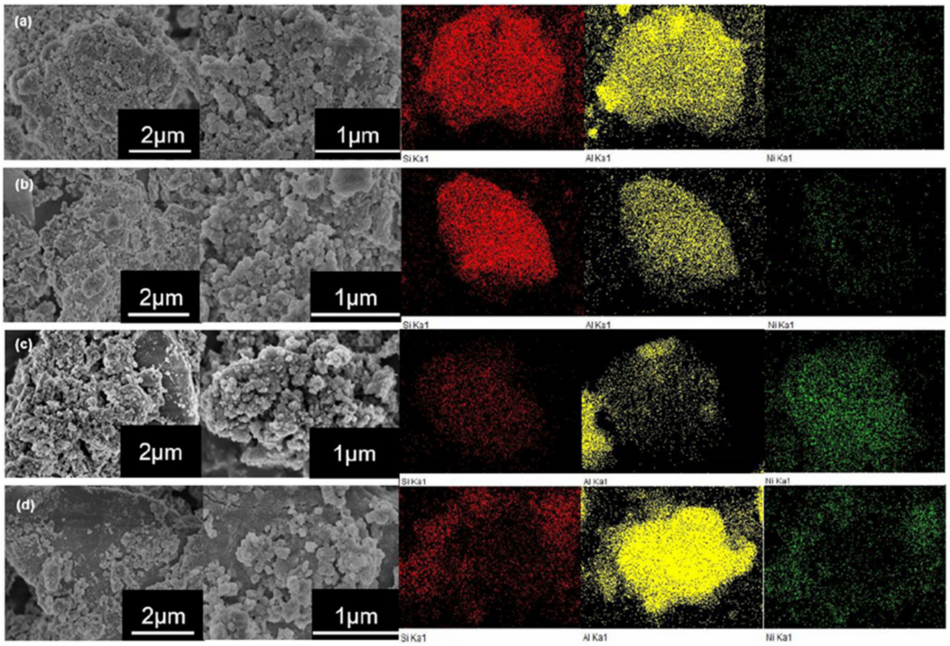

Figure 5. SEM patterns of geopolymer–type zeolite–like products derived from different raw materials. (**a**) NiO–GC–MK7, (**b**) NiO–GC–WIFA, (**c**) NiO–GC–SPS, (**d**) NiO–GC–PFPS.

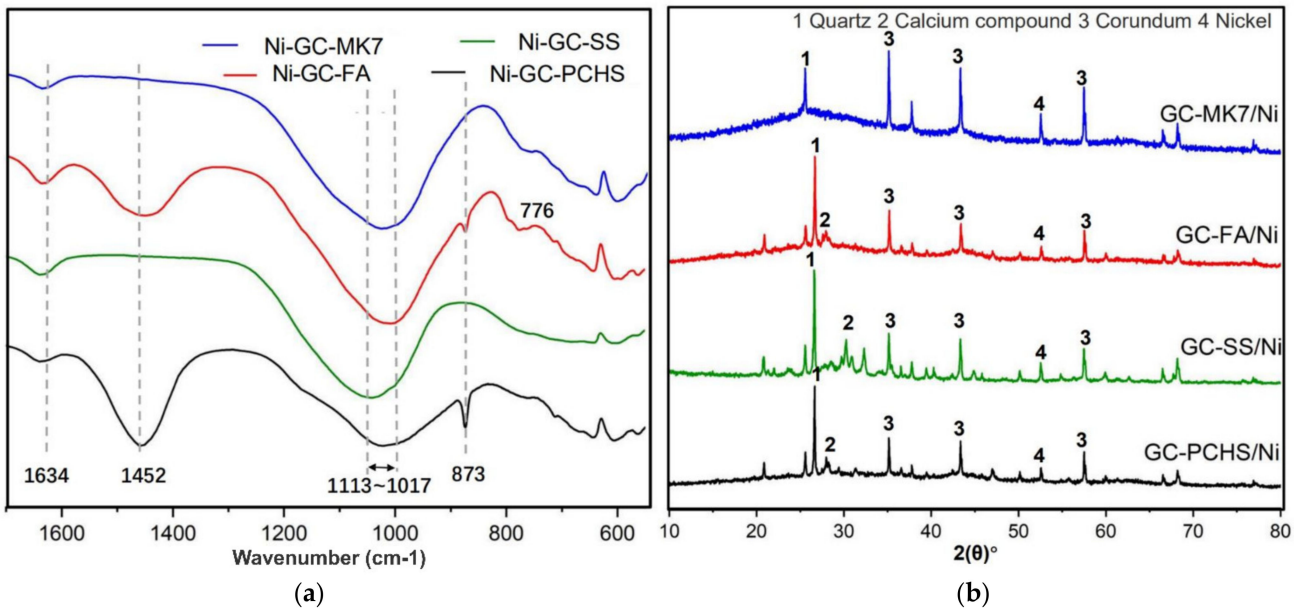

Figure 6. (**a**,**b**) FTIR and XRD patterns of NiO–GC–MK7, NiO–GC–WIFA, NiO–GC–SPS, and NiO–GC–PFPS, respectively.

Table 2. Chemical composition (%) of raw materials by XRF analysis.

Name	SiO_2 (%)	Al_2O_3 (%)	Fe_2O_3 (%)	CaO (%)	MgO (%)	K (%)	Na (%)	S (%)	Cl (%)
WIFA	7.58	3.07	2.46	30.12	1.75	9.68	9.01	3.82	32.79
SPS	33.52	15.89	10.64	9.21	3.32	4.16	1.38	8.25	0.53
PFPS	38.39	11.07	6.73	13.27	2.72	2.28	0.64	2.09	0.11
MK	54.00	43.00	1.00	–	–	–	–	–	–

2.3. Catalyst Performance Evaluation

The above catalysts were subjected to complete reduction and semi–reduction treatments, respectively, and applied to the reaction of converting LA to GVL. First, the catalyst was complete–reduced under traditional restore conditions (550 °C, 3 h, 75% H_2/N_2). Figure 7 shows that the LA conversion rate reached 100% under the set reaction conditions. Both Ni–GC–MK7 and Ni–GC–WIFA have higher GVL yields of 94%. The catalyst was then semi–reduced. Experiments confirm that 500 °C is the best half–reduction temperature for this type of nickel catalyst; the Ni/NiO catalyst prepared by reduction at this temperature has the best catalytic effect. Under the set reaction conditions, the LA conversion rate achieved 100%, and the GVL yields of Ni/NiO–GC–MK7 and Ni/NiO–GC–WIFA were higher, being 98% and 93%, respectively. Compared with the total–reduced nickel catalyst, the catalytic effect of semi–reduced nickel catalyst was improved, which may be related to the formation of the Ni/NiO heterojunction. Previous studies showed that the formation of an Ni/NiO heterojunction is helpful in improving the catalytic activity of an Ni catalyst [32]. Considering the energy consumption and catalytic performance comprehensively, 500 °C semi–reduction was selected as the optimal preparation condition for the catalyst. In summary, the effects of solid waste–derived nickel catalysts and metakaolinite–derived nickel catalysts are comparable, indicating that the developed synthesis strategy is suitable for using solid wastes as raw materials. According to Figure 7 and Table 3, the catalytic effect of Ni/NiO–GC–WIFA is the best, which is comparable to those prepared by commercial carriers, indicating that this product could be used in various catalytic fields instead of commercial catalytic carriers.

Table 3. Comparison of the results of this study with the nickel catalysts reported in the literature and their application in the production of GVL.

Support	Active Metal	Reaction Conditions	Yield	Reference
None	Ni	250 °C, 150 min	93%	[33]
None	Ni/NiO	120 °C, 120 min	>99%	[32]
γ–Al_2O_3	Ni (15 wt%)	200 °C, 240min	92%	[34]
SiO_2	Ni (50%)	200 °C, 60 min	40%	[20]
HZSM–5	Ni (5 wt%)	210 °C, 120 min	100%	[18]
Carbon nanotubes	Ni (10 wt%)	180 °C, 360 min	>90%	[23]
Zeolite materials	Ni (10 wt%)	200 °C, 180 min	94%	this work (maximum)
Zeolite materials	Ni/NiO (10 wt%)	200 °C, 240 min	98%	this work (maximum)

Combined with the previous results and Table 2 in Section 2.2, it was found that raw materials rich in silicon, aluminum, or a certain amount of calcium, are ideal raw materials for the preparation of geopolymer–type zeolite–like products, while the excessive residual moisture or carbon content in raw materials will damage the structure of synthetic materials.

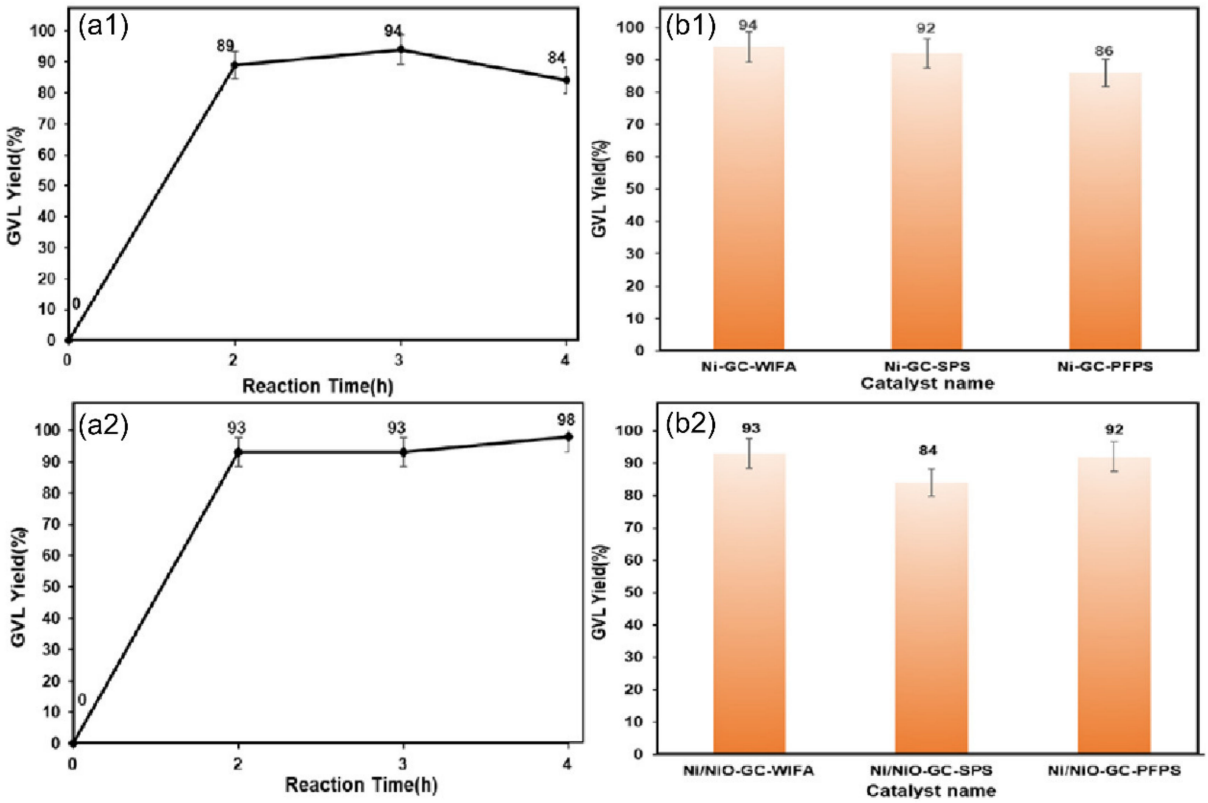

Figure 7. (**a1**,**b1**) 0.5 g Ni–GC–MK7 and 0.5 g Ni/NiO–GC–MK7, respectively; other conditions are the same: 1 mL levulinic acid, 10 mL isopropanol, 200 °C, 2~4 h reaction times, initial hydrogen pressure 4 Mpa, 800 rpm. (**a2**,**b2**) Ni and Ni/NiO catalysts derived from WIFA, SPS and PFPS solid wastes; the reaction time is fixed based on the above Ni catalytic experiment best results (3 h of Ni–type catalyst and 4 h of Ni/NiO–type catalyst) to form a catalytic performance comparison with the Ni catalyst; other reaction conditions unchanged.

2.4. Catalyst Repeatability Test

To investigate the stability and reusability of the catalyst, a recovery test was performed. The used catalyst was collected by centrifugation, washed, filtered twice with ethanol and deionized water, and dried at 80 °C overnight. After each catalyst cycle, the catalysts were calcined at 550 °C and subjected to semi–reduction treatment at 500 °C. The results show that the catalyst has good reusability and stability. After four cycles under the same reaction conditions, the activity of the catalyst did not decrease significantly. At the fifth cycle, the yields of GVL decreased by 3.82% and 1.23%, 2.29%, and 33.50%, respectively, which can be seen in Table 4, the catalytic performance of Ni/NiO–GC–PFPS decreased most obviously. The FTIR characterization of the catalyst after five cycles of experiments shows at Figure 8, observing the image, it can be found that the vibration of the Si–O–Si peak near 1600 cm^{-1} is weakened, and the Al–O and Si–O peaks near 1400 cm^{-1} disappear, indicating that structural materials may be damaged to some extent; this is also the reason for the decreased catalytic performance. The significant decline of the catalytic performance of Ni/NiO–GC–PFPS may be related to the severe damage to their structure, due to the support GC–PFPS containing a large number of carbonic acid compounds, which weakens the stability and strength of the material.

Table 4. The catalytic effect of the catalyst after five cycle tests.

Catalyst	Reaction Conditions	Conversion	Yield
Ni/NiO–GC–MK7	200 °C, 240 min	100.00%	94.18%
Ni/NiO–GC–WIFA	200 °C, 240 min	100.00%	91.77%
Ni/NiO–GC–SPS	200 °C, 240 min	100.00%	81.71%
Ni/NiO–GC–PFPS	200 °C, 240 min	100.00%	58.50%

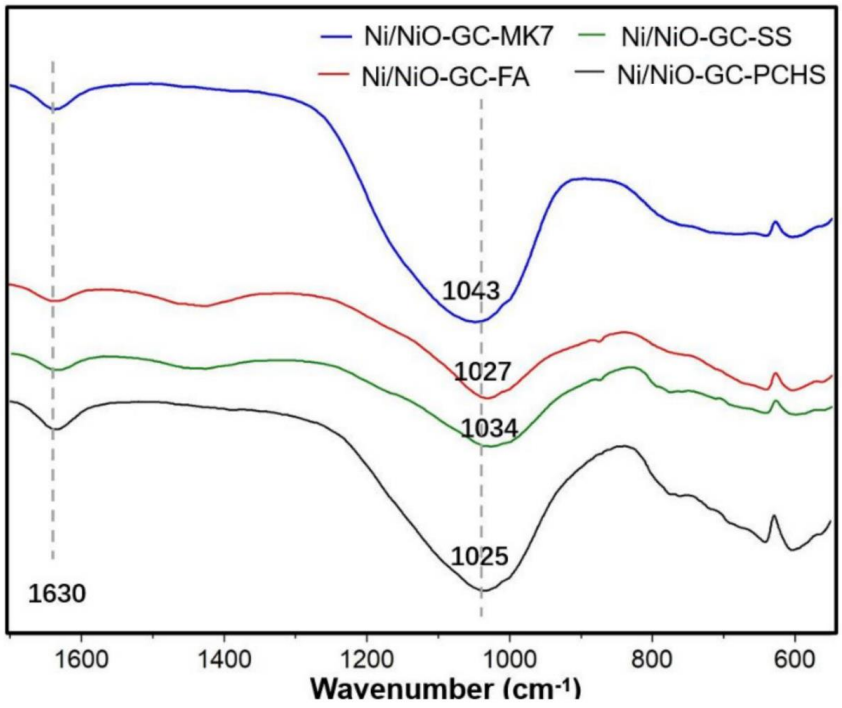

Figure 8. FTIR patterns of Ni/NiO–GC–MK7, Ni/NiO–GC–WIFA, Ni/NiO–GC–SPS, Ni/NiO–GC–PFPS.

2.5. Metal Leaching Test in Reaction Solution

To explore the immobilization of impurities in solid waste by geopolymer–type zeolite–like products, heavy metal leaching experiments were performed. The Ni/NiO catalysts derived from the above three kinds of solid wastes were recycled five times under the optimal reaction conditions (200 °C, 4 h), and the concentration of typical polluting heavy metals (Cu, Zn, Pb, Cd) in the final reaction solution was tested by ICP. The test results are shown in Table 5. The results show that the geopolymer–type zeolite–like product has a good fixation effect on impurities, such as heavy metals, in solid waste, and the leaching amounts of heavy metals are all lower than the limit value of the comprehensive sewage discharge standard GB8978–1996 (Class I Standard). Therefore, the solid–waste–derived geopolymer zeolite not only possesses good structural characteristics, but also demonstrates good heavy metal fixation and stability, and can resist extreme environmental interference, such as high temperature and pressure, demonstrating very good application potential.

Table 5. Typical heavy metal standard limits and heavy metal concentrations in reaction solution (ICP test) (mg/L).

Test Element	WIFA	PFPS	SPS	Standard Limit Value (Class I Standard of GB8978–1996)
Cu	0.045	0.26	0.027	≤0.5
Zn	0.348	1.988	0.149	≤2
Pb	0.151	0.097	0.004	≤1
Cd	–	–	0.001	≤0.1

3. Materials and Methods

3.1. Materials

WIFA was sourced from the Shengyun Environmental Protection Power Co., Ltd in Lhasa, China, SPS was sourced from the Dongjiao Sewage Treatment Plant in Tianjin, China, PFPS was sourced from the Jinyu Zhenxing Environmental Protection Technology Co., Ltd., in Tianjin, China, and MK was purchased from Haofu Chemical. The main chemical properties are shown in Table 1. Potassium silicate (K_2SiO_3, AR, anhydrous grade), potassium hydroxide (KOH, 95%), alumina (Al_2O_3, AR), oleic acid solution ($C_{18}H_{34}O_2$, 99%), LA ($C_5H_8O_3$, 99%), and isopropanol $(CH_3)_2CHOH$, ≥99.7%) were supplied by rhawn; Ni nitrate hexahydrate (NiN_2O_6 $6H_2O$, AR, 98%) was obtained from Aladdin; hydrogen peroxide solution (H_2O_2, 30%, analytical grade) was obtained from Jiangtian Chemical in Nantong, China.

3.2. Material Preparation

First, the geopolymer–type zeolite–like product was prepared using MK as the raw material for the control experiments, and the synthesis strategy and material structure were optimized by adjusting the dosage and ratio of exogenous reagents. The first step was alkali activation. The total amount of alkali activator was determined to be 80 wt% of the raw material mass, and the alkali activator was composed of KOH (11 mol/L) and K_2SiO_3 (28 wt%) solution. Several parallel experiments were then designed by varying the alkali activation conditions, as follows: (1) The ratios (v/v) of K_2SiO_3 to KOH were adjusted to 0.9:1, 1:1, 1:0.9; (2) The total amount of KOH (11 mol/L) was maintained as 40 wt% of the raw material quality; (3) The amount of K_2SiO_3 added was adjusted to be 50 wt%, 60 wt%, 70 wt%, and 80 wt% of the raw material mass, respectively. After the addition of the reagents, the obtained mixtures were stirred at room temperature for 20 min to obtain a slurry following the alkali activation. Alumina with a raw material mass of 15 wt% was added to the slurry as a binder, and the mixture was fully stirred; this was pre–cured at 80 °C for 10 min. The second step was to conduct direct foaming. Diluted hydrogen peroxide (3%) and pure oleic acid were added to the pre–cured slurry for foaming. The dropwise addition conditions were as follows: dropwise in turn while stirring. The foaming effect was best (the foam was fine and uniform) when it was 260 wt% and 40 wt% of the raw material quality. Subsequently, the obtained foamed product was cured at 80 °C for 48 h to form an inorganic gel foam. The foam was fully ground into fine powder, then put in a furnace and calcined in the flowing air at 550 °C for 3 h until the residues of organic compounds such as oleic acid were fully burned off. This produced the geopolymer–type zeolite–like control materials. These new materials, synthesized under the different alkali activation conditions, were named GC–MK1~GC–MK7, in turn.

Based on the optimized synthesis conditions of the geopolymer–type zeolite–like control product in the above experiments, this material was then synthesized using different solid wastes as the raw materials. The solid wastes were: waste incineration fly ash, sewage plant sludge, and high–pollution soil from pesticide plants following high temperature treatment. The sewage sludge was dried and pulverized, and all solid wastes were passed through a 200–mesh sieve. The geopolymer–type zeolite–like material synthesized from different solid wastes were named GC–WIFA, GC–SPS and GC–PHCS, respectively.

3.3. Catalyst Preparation

The non–precious metal hydrogenation catalyst was prepared using the ultra–wet impregnation method, and the Ni loading was controlled to be about 10 wt%. The geopolymer–type zeolite–like products synthesized from the different raw materials were used as catalyst precursors. The precursor materials were added to $Ni(NO_3)_2 \cdot 6H_2O$ aqueous solution, stirred at room temperature for 12 h, filtered and washed with pure water 3 times, and dried at 80 °C, 10 h. After drying, the powder was calcined at 550 °C for 4 h in flowing air, and then reduced for 3 h at 550 °C under 75% H_2/N_2 flow conditions to prepare the Ni–based catalyst [17]. The Ni/NiO–based catalysts were prepared by reduction under the following conditions for 1 h [32]: 300~500 °C, 75~500 °C, and 75% H_2/N_2 flow conditions.

3.4. Characterization Test

Carrier and catalyst were characterized by N_2 adsorption–desorption studies, FTIR, XRD, SEM, and SEM–EDS. The N_2 adsorption–desorption isotherm studies were performed using a Mic ASA P2460 surface area analyzer at liquid nitrogen temperature (77 K) to determine the BET surface area. The infrared spectra of the synthesized materials were recorded using an Nicolet iS10 FTIR spectrometer from Thermo Fisher Scientific, Waltham, MA, USA, and the samples were mixed with KBr at a ratio of 1:50 wt% in the range of 400~4000 cm^{-1} with a resolution of 4 cm^{-1}. XRD measurements were performed using a Bruker D8 Advance X–ray diffractometer at 40 kV and 40 mA using monochromatic CuK α radiation (k = 1.5406 Å). The detailed imaging information of the sample topography and surface texture was obtained using a Hitachi SU8020 high–resolution field emission scanning electron microscope (SEM) and SEM–EDS under the condition of operating voltage of 3 kV and 10 mA. The reaction progress was monitored by gas chromatography (SP–7890) and gas chromatography–mass spectrometry (6890A–5975 C, Agilent, Santa Clara, CA, USA) equipped with an InertCap 5 column (30 m × 0.32 mm × 0.25 μm, Shimadzu, Kyoto, Japan) and a flame ionization detector.

3.5. Catalytic Reaction Experiments

The catalytic hydrogenation of LA was carried out in a 25 mL stainless steel batch autoclave. In a typical run, the autoclave was loaded with catalyst (0.5 g), LA (1.13 g), and isopropanol (10 mL) with an initial hydrogen pressure of 4 MPa. The reactor was then heated to the setpoint temperature at a constant stirring rate of 800 rpm. Qualitative and quantitative analysis of GVL and other reaction products by gas chromatography (SP–7890) and gas chromatography–mass spectrometry (6890 A–5975 C, Agilent) using an InertCap 5 column (30 m 0.32 mm 0.25 μm, Shimadzu) and flame ionization detector. After the reaction, the solid residue was washed and filtered twice with ethanol and deionized water, respectively, then dried at 80 °C overnight, calcined at 550 °C for 4 h, and reduced under certain conditions for use in the next cycle (the restore conditions were the same as those in Section 3.3).

4. Conclusions

A method for synthesizing geopolymer–type zeolite–like high–functional materials from cheap and readily available solid waste was developed, an optimized synthesis strategy was obtained, and the effects of different raw materials on the properties of synthetic materials were studied. The results show that:

1. Raw materials with a high content of silicon, aluminum, or calcium, such as waste incineration fly ash, are ideal raw materials for synthesizing geopolymer zeolite.
2. The optimal synthesis conditions are as follows: the proportion of alkali activator is 40 wt% KOH solution (11 mol/L) and 70~80 wt% K_2SiO_3 solution (99%); the proportion of foaming agent is 3%. The total amount accounts for about 350% of the total amount of raw materials, and the mixing ratio of hydrogen peroxide (3%) and the foam stabilizer (pure oleic acid solution) is about 6.5:1 (*w*/*w*).

3. The geopolymer–type zeolite synthesized under the above conditions possesses good structural properties and is suitable as a carrier to prepare a nickel catalyst. Ni/NiO–GC–WIFA can achieve a 100% LA conversion and a 94% GVL yield, with the GVL yield only decreasing by 1.23% after five cycles.
4. The characterization test results show that the geopolymer–type zeolite–like product prepared using this method possesses excellent pore and surface structure, and high stability and durability. The catalytic effect of the catalyst prepared with the geopolymer–type zeolite–like product as a carrier is similar to that of the catalyst prepared with a typical commercial carrier. In the future, this material is also expected to be used in various high–value fields, such as electrocatalysis and adsorption.

Author Contributions: Conceptualization, W.F. and X.L.; methodology, R.Z.; software, J.C.; validation, Y.W., W.F.; formal analysis, R.W., Z.Y.; investigation, W.F.; resources, W.F.; data curation, J.X.; writing—original draft preparation, W.F.; writing—review and editing, R.Z.; visualization, R.W.; supervision, R.Z.; project administration, X.L.; funding acquisition, X.L. All authors have read and agreed to the published version of the manuscript.

Funding: This research was funded by [National Natural Science Foundation of China] grant number [51908400, 52066017, 51876180] and The Mount Everest Discipline Construction Project was funded by [Tibet University].

Conflicts of Interest: The authors declare no conflict of interest.

References

1. Li, Q.; Faramarzi, A.; Zhang, S.; Wang, Y.; Hu, X.; Gholizadeh, M. Progress in catalytic pyrolysis of municipal solid waste. *Energy Convers. Manag.* **2020**, *226*, 113525. [CrossRef]
2. Nanda, S.; Berruti, F. Municipal solid waste management and landfilling technologies: A review. *Environ. Chem. Lett.* **2020**, *19*, 1433–1456. [CrossRef]
3. Kaya-Özkiper, K.; Uzun, A.; Soyer-Uzun, S. Red mud- and metakaolin-based geopolymers for adsorption and photocatalytic degradation of methylene blue: Towards self-cleaning construction materials. *J. Clean. Prod.* **2021**, *288*, 125120. [CrossRef]
4. Huang, B.B.; Gan, M.; Ji, Z.Y.; Fan, X.H.; Zhang, D.; Chen, X.L.; Sun, Z.Q.; Huang, X.X.; Fan, Y. Recent progress on the thermal treatment and resource utilization technologies of municipal waste incineration fly ash: A review. *Process Saf. Environ. Prot.* **2022**, *159*, 547–565. [CrossRef]
5. Ren, B.; Zhao, Y.L.; Bai, H.Y.; Kang, S.C.; Zhang, T.T.; Song, S.X. Eco-friendly geopolymer prepared from solid wastes: A critical review. *Chemosphere* **2021**, *267*, 128900. [CrossRef]
6. Rożek, P.; Król, M.; Mozgawa, W. Geopolymer-zeolite composites: A review. *J. Clean. Prod.* **2019**, *230*, 557–579. [CrossRef]
7. Missengue, R.N.M.; Losch, P.; Sedres, G.; Musyoka, N.M.; Fatoba, O.O.; Louis, B.; Pale, P.; Petrik, L.F. Transformation of South African coal fly ash into ZSM-5 zeolite and its application as an MTO catalyst. *C. R. Chim.* **2017**, *20*, 78–86. [CrossRef]
8. Vichaphund, S.; Wimuktiwan, P.; Sricharoenchaikul, V.; Atong, D. In Situ catalytic pyrolysis of Jatropha wastes using ZSM-5 from hydrothermal alkaline fusion of fly ash. *J. Anal. Appl. Pyrolysis* **2018**, *139*, 156–166. [CrossRef]
9. De Oliveira, L.B.; de Azevedo, A.R.; Marvila, M.T.; Pereira, E.C.; Fediuk, R.; Vieira, C.M.F. Durability of geopolymers with industrial waste. *Case Stud. Constr. Mater.* **2022**, *16*, e00839. [CrossRef]
10. Bai, C.; Colombo, P. Processing, properties and applications of highly porous geopolymers: A review. *Ceram. Int.* **2018**, *44*, 16103–16118. [CrossRef]
11. Farooq, F.; Jin, X.; Javed, M.F.; Akbar, A.; Shah, M.I.; Aslam, F.; Alyousef, R. Geopolymer concrete as sustainable material: A state of the art review. *Constr. Build. Mater.* **2021**, *306*, 124762. [CrossRef]
12. Shehata, N.; Sayed, E.T.; Abdelkareem, M.A. Recent progress in environmentally friendly geopolymers: A review. *Sci. Total Environ.* **2021**, *762*, 143166. [CrossRef] [PubMed]
13. Bai, C.; Ni, T.; Wang, Q.; Li, H.; Colombo, P. Porosity, mechanical and insulating properties of geopolymer foams using vegetable oil as the stabilizing agent. *J. Eur. Ceram. Soc.* **2018**, *38*, 799–805. [CrossRef]
14. Kaewmee, P.; Song, M.; Iwanami, M.; Tsutsumi, H.; Takahashi, F. Porous and reusable potassium-activated geopolymer adsorbent with high compressive strength fabricated from coal fly ash wastes. *J. Clean. Prod.* **2020**, *272*, 122617. [CrossRef]
15. Yu, Z.; Lu, X.; Liu, C.; Han, Y.; Ji, N. Synthesis of γ-valerolactone from different biomass-derived feedstocks: Recent advances on reaction mechanisms and catalytic systems. *Renew. Sustain. Energy Rev.* **2019**, *112*, 140–157. [CrossRef]
16. Omoruyi, U.; Page, S.; Hallett, J.; Miller, P.W. Homogeneous Catalyzed Reactions of Levulinic Acid: To γ-Valerolactone and Beyond. *ChemSusChem* **2016**, *9*, 2037–2047. [CrossRef]
17. Xu, W.P.; Chen, X.F.; Guo, H.J.; Li, H.L.; Zhang, H.R.; Xiong, L.; Chen, X.D. Conversion of levulinic acid to valuable chemicals: A review. *J. Chem. Technol. Biotechnol.* **2021**, *96*, 3009–3024. [CrossRef]

18. Zhang, D.; Zhao, Y.-P.; Fan, X.; Liu, Z.-Q.; Wang, R.-Y.; Wei, X.-Y. Catalytic Hydrogenation of Levulinic Acid into Gamma-Valerolactone over Ni/HZSM-5 Catalysts. *Catal. Surv. Asia* **2018**, *22*, 129–135. [CrossRef]
19. Dutta, S.; Yu, I.K.M.; Tsang, D.C.W.; Ng, Y.H.; Ok, Y.S.; Sherwood, J.; Clark, J.H. Green synthesis of gamma-valerolactone (GVL) through hydrogenation of biomass-derived levulinic acid using non-noble metal catalysts: A critical review. *Chem. Eng. J.* **2019**, *372*, 992–1006. [CrossRef]
20. Hengne, A.M.; Kadu, B.S.; Biradar, N.S.; Chikate, R.C.; Rode, C.V. Transfer hydrogenation of biomass-derived levulinic acid to γ-valerolactone over supported Ni catalysts. *RSC Adv.* **2016**, *6*, 59753–59761. [CrossRef]
21. Cai, B.; Zhang, Y.; Feng, J.; Huang, C.; Ma, T.; Pan, H. Highly efficient g-C3N4 supported ruthenium catalysts for the catalytic transfer hydrogenation of levulinic acid to liquid fuel γ-valerolactone. *Renew. Energy* **2021**, *177*, 652–662. [CrossRef]
22. Chen, C.-B.; Chen, M.-Y.; Zada, B.; Ma, Y.-J.; Yan, L.; Xu, Q.; Li, W.-Z.; Guo, Q.-X.; Fu, Y. Effective conversion of biomass-derived ethyl levulinate into γ-valerolactone over commercial zeolite supported Pt catalysts. *RSC Adv.* **2016**, *6*, 112477–112485. [CrossRef]
23. Sosa, L.F.; da Silva, V.T.; de Souza, P.M. Hydrogenation of levulinic acid to γ-valerolactone using carbon nanotubes supported nickel catalysts. *Catal. Today* **2021**, *381*, 86–95. [CrossRef]
24. Panias, D.; Giannopoulou, I.P.; Perraki, T. Effect of synthesis parameters on the mechanical properties of fly ash-based geopolymers. *Colloids Surf. A Physicochem. Eng. Asp.* **2007**, *301*, 246–254. [CrossRef]
25. Hajimohammadi, A.; Ngo, T.; Mendis, P.; Nguyen, T.; Kashani, A.; van Deventer, J.S. Pore characteristics in one-part mix geopolymers foamed by H_2O_2: The impact of mix design. *Mater. Des.* **2017**, *130*, 381–391. [CrossRef]
26. Falliano, D.; De Domenico, D.; Ricciardi, G.; Gugliandolo, E. Key factors affecting the compressive strength of foamed concrete. *IOP Conf. Ser. Mater. Sci. Eng.* **2018**, *431*, 062009. [CrossRef]
27. Hou, L.; Li, J.; Lu, Z.; Niu, Y. Influence of foaming agent on cement and foam concrete. *Constr. Build. Mater.* **2021**, *280*, 122399. [CrossRef]
28. Su, Y.; Wei, B.; Sun, X.; Zhang, H. Factors affecting the stability of bubble in autoclaved aerated concrete. *ce/papers* **2018**, *2*, 181–186. [CrossRef]
29. Kim, B.; Lee, S. Review on characteristics of metakaolin-based geopolymer and fast setting. *J. Korean Ceram. Soc.* **2020**, *57*, 368–377. [CrossRef]
30. Kovalchuk, G.; Fernández-Jiménez, A.; Palomo, A. Alkali-activated fly ash: Effect of thermal curing conditions on mechanical and microstructural development—Part II. *Fuel* **2007**, *86*, 315–322. [CrossRef]
31. Somna, K.; Jaturapitakkul, C.; Kajitvichyanukul, P.; Chindaprasirt, P. NaOH-activated ground fly ash geopolymer cured at ambient temperature. *Fuel* **2011**, *90*, 2118–2124. [CrossRef]
32. Song, S.; Yao, S.; Cao, J.; Di, L.; Wu, G.; Guan, N.; Li, L. Heterostructured Ni/NiO composite as a robust catalyst for the hydrogenation of levulinic acid to γ-valerolactone. *Appl. Catal. B Environ.* **2017**, *217*, 115–124. [CrossRef]
33. Zhong, H.; Li, Q.; Liu, J.; Yao, G.; Wang, J.; Zeng, X.; Huo, Z.; Jin, F. New Method for Highly Efficient Conversion of Biomass-Derived LevuliNic Acid to γ-Valerolactone in Water without Precious Metal Catalysts. *ACS Sustain. Chem. Eng.* **2017**, *5*, 6517–6523. [CrossRef]
34. Hengst, K.; Schubert, M.; Carvalho, H.W.P.; Lu, C.; Kleist, W.; Grunwaldt, J.-D. Synthesis of γ-valerolactone by hydrogenation of levuliNic acid over supported Nickel catalysts. *Appl. Catal. A General* **2015**, *502*, 18–26. [CrossRef]